Damage monitoring of carbon fibre reinforced polymer composites using acoustic emission technique and deep learning

DAMAGE MONITORING OF CARBON FIBRE REINFORCED POLYMER COMPOSITES USING ACOUSTIC EMISSION TECHNIQUE AND DEEP LEARNING

Claudia Barile [a]*, Caterina Casavola [a], Giovanni Pappalettera [a], Vimalathithan Paramsamy Kannan [a]

[a] *Dipartimento di Meccanica Matematica e Management, Politecnico di Bari, Via Orabona 4, 70125 – Bari*

Paper submitted for publication in

Composite Structures

**Author to whom the correspondence to be addressed*

Dr. Claudia Barile

Dipartimento di Meccanica, Matematica e Management

Politecnico di Bari, Via Orabona 4 - 70125 Bari, Italy.

Email ID: claudia.barile@poliba.it

DAMAGE MONITORING OF CARBON FIBRE REINFORCED POLYMER COMPOSITES USING ACOUSTIC EMISSION TECHNIQUE AND DEEP LEARNING

Claudia Barile [a]*, Caterina Casavola [a], Giovanni Pappalettera [a], Vimalathithan Paramsamy Kannan [a]

[a] *Dipartimento di Meccanica Matematica e Management, Politecnico di Bari, Via Orabona 4, 70126 – Bari*

Abstract

In this research work, a deep Convolutional Neural Network (CNN) was trained for image-based Acoustic Emission (AE) waveform classification. AE waveforms from different damage modes of Carbon Fibre Reinforced Polymer (CFRP) composites were used to train the CNN for online damage monitoring. Spectrograms of AE Waveforms from four different damage modes, matrix cracking, delamination, debonding, and fibre breakage, were obtained in their Mel scale and used as the training data and test data for the CNN. The overall prediction accuracy of the CNN is 97.9%, while the fibre breakage and delamination events were able to be predicted with 100% accuracy. Then this pre-trained CNN is used for online damage monitoring of mode I delamination test of CFRP specimens. AE waveforms generated during the mode I test are classified using the trained CNN and the results are analysed in terms of the classified AE descriptors. The classified AE descriptors proved to identify the occurrences of different damage modes, thereby validating the damage classification accuracy of the CNN.

Keywords: Acoustic Emission; Convolutional Neural Network (CNN); Deep Learning; Online damage monitoring; CFRP

1. Introduction

Fibre Reinforced Polymer (FRP) composites have revolutionized the industrial sector in the past few decades. They have replaced most of the conventional materials used in many industrial and commercial applications. Due to their extraordinary strength-to-weight ratio and stiffness-to-weight ratio, they are preferred over metals in variety of applications. Despite the tremendous interest it has garnered among the industrialists and academician, the failure prediction and tracking of damage evolution in FRP have not reached their pinnacle [1-3]. Needless to say, several attempts have been made till date to transfer the concepts of failure predictions in conventional engineering materials to these heterogeneous and anisotropic materials [4-7].

Several Non-Destructive Evaluation (NDE) tools have been developed over the years for online monitoring of FRP composites and their structures; one among them is Acoustic Emission (AE) technique. AE technique is a passive NDE tool, which can quantitatively predict the failures and the modes of failure in FRP. AE technique is based on the principle that the elastic waves are generated within a material when the said material undergoes damage and irreversible deformation [7-10]. The characteristics of the elastic waves generated vary significantly based on their source. For instance, in an FRP, the different damage modes such as matrix cracking, delamination, debonding and fibre breakage generate AE waves which vary in their time-frequency domain [7, 9 & 11]. The characteristics of these waveforms can be traced back to their sources. This essentially bridges the gap in predicting the failure or tracking the damage evolution in FRP.

Research works dated from the late 1960s have aimed at maximizing the potential of AE in failure prediction and characterizing the modes of damage evolution [7 & 12]. In the past decade, several researchers have validated the frequency characteristics of AE waves generated from different damage modes. Groot et al. have designed Carbon Fibre Reinforced Polymer (CFRP) composites to fail at different damage modes and analysed the AE waves generated from these damage modes [13]. They have concluded that AE waves from matrix cracking has a frequency of about 90 kHz – 180 kHz, fibre breakage above 300 kHz, fibre pull-out 180 kHz – 240 kHz and debonding 240 kHz – 310 kHz. Oz et al. have experimentally validated that the high frequency AE waves (generally above 300 kHz) are not only generated from fibre breakage event but also from through-thickness crack growths [11]. Several research works have corroborated with these frequency analyses, especially in the last 2 decades. The consensus is that analysing an acoustic signal in their frequency domain, or their time-frequency domain is more advantageous than using parameter-based data such as amplitude, duration, etc. Nonetheless, a definite online monitoring tool for predicting and validating the damage modes in FRP/CFRP is still in progress [7, 9 & 14].

Image-based deep learning has been integrated into AE technique only in the very recent years. The incorporation of image-based deep learning has been used in predicting the corrosion rate of steel [15], ultrasonic image detection for classifying damages in CFRP [17] and monitoring cracks in civil structures [14]. Nonetheless, deep learning in AE specifically for AE waveform classification can be seldom found in literature. Recently, Nasiri et al. [17] and Lin et al. [19] have used deep learning for detecting damages in ceramic composites and structural damages, respectively. Khan et al. designed a deep learning neural network for classifying and predicting the in-plane and through-thickness delamination in laminated

composites through the low-frequency vibrational signals from the structures [20]. Sikdar et al. have used CWT for extracting damage features from CFRP structures, however, the image augmentation is used in their research work for generating training data [21]. Besides, 1-D waveforms or Wavelet Packets of the AE waves have been used for image classification in these research works [15-21].

In this research work, Convolutional Neural Network (CNN) based deep learning model is created for classifying the AE waves generated from different damage modes in CFRP test specimens. Among the other deep learning networks, CNN is the one that is less dependent on pre-processing and requires less attention in developing the functionalities. The time-frequency representations of the AE waveforms in their Mel spectrogram are used as the training and test dataset for developing and validating the model, respectively. To our best knowledge, this is the first-time image-based deep learning model is developed for classifying damage modes in CFRP using AE waveforms. Moreover, this is the first time Mel spectrograms are used for this defined purpose.

2. Deep Convolutional Neural Network

Convolutional Neural Networks (CNN) combine the ideas of local receptive fields, shared weights, and spatial sub-sampling to ensure some degree of shift, scale, and distortion invariance in input images. It is preferred over Artificial Neural Networks (ANN) due to their greater efficiency in solving classification problems. Besides, ANN can be used only for data classification and not for image-based classification. Some researchers have used ANN for characterizing damage modes in composites using AE data, but very limited research works have used image-based classification [21 & 22].

A typical CNN consists of an input layer, an output layer and several hidden layers. Mostly, the hidden layers include convolutional layer, pooling layer, fully connected layer, and softmax layer. For waveform-based image processing, the input layer receives time-series based inputs or spectrograms as input. The definitions of different layers within a CNN network, their architecture, and the functions such as padding, stride, etc. are enriched in textbooks and several research works [23 & 24]. This section is dedicated to the CNN architecture developed for this research work and detailed information on the input data used for training the network.

2.1 Architecture of the CNN

The CNN built for this study has an input layer, classification layer and 9 hidden layers. It consists of 3 convolutional layers, each of their output is sorted by a pooling layer and an activation function. The output of the first convolutional layer (Convolution 1) is followed by a maximum pooling layer and is activated through a ReLu activation function. The outputs of the other convolutional layers (Convolution 2 and Convolution 3) are followed by average pooling layers and activated through ReLu functions. The pooling layer extracts the most representative features of the convolutional output by striding and padding operations. The maximum pooling layer is used to extract the features with the most activated presence from the output of Convolution 1 layer. For the outputs of the subsequent convolutional layers, average pooling layer is used for extracting a smooth generalized number of features. ReLu activation function is preferred over sigmoid or tanh functions because of its non-saturation of gradients, which improves the convergence of stochastic gradient [25]. The details about the kernel size, padding and stride of the convolutional layers and the pool size, padding and stride of the pooling layers are presented in Table 1. In addition to that, the details about the other layers and the detailed architecture are presented in Figure 1.

Figure 1. Architecture of the Convolutional Neural Network

While training the CNN network, the error functions must be minimized. For minimizing the error functions, the weights of the different layers must be assigned. Weights for the convolutional layers and the fully connected layers are predefined for the network built in this study. Initialization of weights is crucial for the algorithm to converge. The algorithm may encounter numerical difficulties in convergence and fail when the weights are not properly initialized [26]. Generally, weights can be initialized in two ways: zero initialization and random initialization. He et al. proposed a method for initializing weights, which radically can improve the efficiency of training the CNN network, which is popularly called as He initialization. According to He initialization [27], the randomly initialized weights assigned must be multiplied by a function, which is given in Equation (1).

$$\sqrt{\frac{2}{Size^{[l-1]}}} \tag{1}$$

where, l is the previous layer. In this research work, the weights are assigned based on He initialization. For training the CNN network, Stochastic Gradient Descent (SDG) algorithm is used. The initial learning rate is set to 0.001 with a 'piecewise' learn rate schedule and learn rate drop factor of 0.1. A total of 20000 input images are fed to the model

with a batch size of 50 and maximum number of epochs 20. The CNN model is built and trained using Machine Learning and Deep Learning toolbox in MATLAB® [28 & 29].

Table 1. Configuration of the Proposed CNN model

2.2 Input data for CNN training and testing

For waveform-based image classification training, the input is either fed as the time-series data or as spectrograms. In this research work, the latter is used as the training input. The waveforms are processed in their Mel frequency bands. The spectrograms are produced, which are then used as the training and testing data of the CNN. Mel spectrograms are popularly used in many auditory applications, especially in the field of music pattern recognitions and voice recognition [30-32]. Only in the recent years, Mel scale have found its way into the field of health monitoring using AE technique [33 & 34]. Mel spectrograms scale down the signal into human auditory frequency range. A human auditory system recognises sounds in a logarithmic scale. Therefore, more spectral components can be extracted from a signal with narrow frequency bands, when they are scaled down into Mel scale. This is why the Mel spectrograms have proven to be very efficient in classifying sound wave-based waveforms. Since AE itself is nothing more than a sound wave in a solid medium, it is used. In this study, the waveforms required for training and testing are first scaled down to 22 kHz and the Mel spectrograms are obtained with the window length of 64 and overlap length of 16. Since Mel scale works more efficiently in human auditory frequency range, all the AE waveforms are scaled down to 22 kHz. The choice of window length and the overlapping length is to extract the most significant spectral content from the AE waveforms without losing much information.

In our previous studies, the AE waveforms generated from different damage modes in CFRP test specimens were identified using Wavelet Packet Transform (WPT) [14]. The waveforms classified from our previous studied are used as both the training and test data for CNN built in this study. The Mel spectrograms of the representative waveforms generated from matrix cracking, delamination, debonding and fiber breakage events are presented in Figure 2.

Figure 2. Mel Spectrograms of representative waveforms from Matrix Cracking, Delamination, Debonding and Fibre Breakage events

For training the CNN, a total of 5000 waveforms are selected for each damage mode and are used as the training data, making a total of 20000 waveforms. For testing, another batch

of 20000 waveforms are used. The results of the training and testing of the CNN are presented in the subsequent sections.

3. Damage Characterization using Deep Learning

After training the deep convolutional neural network, it is used for damage characterization in three CFRP test specimens tested under mode I delamination. It must be understood that the propagation of the acoustic waves is affected by the geometrical boundaries and properties of the material [35]. Therefore, for characterizing a material using CNN, it is essential to train the model using the data obtained from similar material; for instance, CFRP laminate manufactured from a similar prepreg using same curing conditions.

3.1 Test Material and Setup

In this research work, the damage modes of CFRP unidirectional test specimens are analysed using the CNN. The CFRP specimens in Double Cantilever Beam (DCB) configuration are prepared as per ASTM D5528 configuration [36]. The length, breadth and thickness of the specimen are 125 mm, 25 mm and 3 mm, respectively. A schematic of the test specimen is presented in Figure 3. The test specimens are prepared from prepreg having 35% epoxy resin content and high-strength carbon fibres in 0° oriented along the delamination direction. The nominal thickness of each unidirectional ply is 0.152 mm. The specimens are prepared using Resin Film Infusion (RFI) process. A non-adhesive insert of length 45 mm and thickness of 13 μm is inserted during the curing process to create the pre-crack for initiating the delamination. A pair of piano hinges are glued to the DCB specimen for applying the load. Tensile load is applied at a crosshead displacement of 1 mm/min in an INSTRON servo-hydraulic testing machine to delaminate the DCB specimens in Mode I delamination. Three specimens are tested accordingly, and the acoustic signals generated during their damage progression are recorded using a piezoelectric sensor.

Figure 3. Schematic of the test specimen

A piezoelectric sensor (R30α) with an operating frequency of 150 kHz to 400 kHz is fixed to the surface of the specimen. Silica gel is smeared on the transducing surface of the piezoelectric sensor before it is fixed to the surface for improving the acoustic coupling. AE signals recorded by the sensor are amplified by 40 dB through a 2/4/6 AE preamplifier and filtered through low-pass band filter and high-pass band filter of 1 kHz and 3 MHz, respectively. AE signals are recorded in burst mode of acquisition. The signals corresponding to the individual damage state within the material are recorded. AE

waveforms are recorded at a sampling rate of 1 MHz to achieve the Nyquist sampling frequency of 500 kHz and for a length of 1K. The sampling rate and the length of the recorded waveforms are selected carefully to be the same as the trained CNN model. The waveforms recorded from these test specimens are scaled down to 22 kHz and their spectrograms are classified using the trained deep convolutional neural network.

4. Results and Discussions

4.1 CNN Training and Test Results

As mentioned in Section 2.2, four different classes of waveforms are fed as the training data to the CNN: matrix cracking, delamination, debonding and fibre breakage. The SDG algorithm is used to train the CNN. During the training, when random weights were initialized for the convolutional layer, the minibatch accuracy did not reach 100% even after 200 epochs. After that, the weights were initialized according to He initialization and the network was trained with a minibatch size of 50. The accuracy reaches 100% after 20 epochs.

The test data is now fed to the trained CNN model to validate its accuracy. The confusion matrix obtained from testing the data is presented in Figure 4.

Figure 4. Confusion Matrix of the CNN classifying the damage modes

From the confusion matrix it can be observed that the accuracy of the CNN in identifying the AE waveforms from the delamination and fibre breakage are 100% after testing the data. The accuracy in identifying the other two damage modes, debonding and matrix cracking are 92.7% and 98.9%, respectively. This is probably due to the reason that in some materials undergoing deformation, the matrix cracking and the debonding events releases acoustic waveforms with a frequency of about 150 kHz to 250 kHz, which are localized in a similar time domain. Nonetheless, the loss in accuracy is not significant to fail the CNN. The overall accuracy of the CNN model constructed in this study is 97.9%.

4.2 Damage mode progression in Mode I test

Three mode I specimens are tested as a part of this study, as mentioned in Section 3 and the AE waveforms are collected over the entire loading history of the test specimens. The number of AE waveforms recorded from each study are presented in Table 2.

Table 2. AE waveforms recorded from the CFRP test specimens under Mode I Delamination

The load responses of the test specimens under mode I delamination is presented as a function of the duration of the test in Figure 5. The counts and energy of the AE waveforms are extracted and their respective cumulative values over the entire loading history of each specimen is calculated. They are also plotted along with the load responses of the specimen in Figure 5.

The cumulative counts and cumulative energy of the AE events recorded in the three specimens do not have the same value, albeit not unnaturally. It has been indicated that the acquisition of the acoustic waves by the piezoelectric sensors is based on the labour skill of the sensors' installer [37]. It has been highlighted in several research works that the values of the AE descriptors can vary among the different specimens or structures having same geometrical and layup configuration due to the installation procedures [35 & 38]. It also has been recommended not to compare the specific values of counts, energy or event rate of the AE waves between different specimens.

Figure 5. Load Responses, Cumulative Counts and Cumulative Energy of the Acoustic Events for a) Specimen A, b) Specimen B and c) Specimen C

All the waveforms generated from the specimens A, B and C are classified into their respective damage modes using the pretrained CNN. After classification, the count distribution, cumulative counts, energy, and cumulative energy of the different damage modes are extracted and analysed. The classified AE descriptors of test specimens A, B and C respectively are presented in Figures 6, 7 and 8.

Figure 6. AE descriptors of Specimen A classified using CNN a) Count Distribution b) Cumulative Counts c) Energy Distribution d) Cumulative Energy

Few important aspects of the damage progressions can be observed from Figures 6, 7 and 8. First, the specimen tested in this study is a unidirectional specimen, which is delaminated along the horizontal direction of the fibre orientation. Therefore, the chances of fibre breakage are very low. Second, due to the unidirectional layup, only the improper curing can result in the debonding between the fibres and the matrix of the subsequent layers. Consequently, the counts, energy, cumulative counts leading to the fibre breakage and debonding event is very low considered to the matrix cracking and delamination event.

In Figure 6, specimen A released AE waves with a cumulative count of only 884 due to the debonding events, which is significantly lower than the other damage modes. The failure progression in the material is dominated by the matrix cracking event and delamination event and to some extent, the fibre breakage event. While looking at Figures 6a and 6b, there

were some AE events with larger counts and higher energies occurring at the early stages of loading. These AE events are mostly from the matrix cracking events and 4 delamination events. And if these results are compared with the load responses in Figure 5a, there is a load drop at the early stages of loading. It can be deduced that the initial damage is due to the matrix cracking and a few delamination. While looking at the cumulative counts and energies in Figures 6b and 6c, one can observe that the fibre breakage starts to occur around 100s duration of the test but increases suddenly around 200s before continuing to progress gradually for the entire duration of the test.

Figure 7. AE descriptors of Specimen B classified using CNN a) Count Distribution b) Cumulative Counts c) Energy Distribution d) Cumulative Energy

In specimen B, there are some AE events with higher energies and larger counts from delamination events dominates at the early stage, before 100s duration (Figure 7a and 7c). Comparing these with the load responses in Figure 5b, the load peak can be observed at the same duration. Therefore, unlike specimen A, the major damage leads to the failure in this specimen is due to the delamination event. This can also be observed in Figure 7d, where the cumulative energies of the delamination and matrix cracking events increase sharply around 100s duration, accounting to the same amount. Nonetheless, after this load drop, the damage is dominated by matrix cracking and delamination events (Figures 7b and 7d). The fibre breakage events, and debonding events play a very minor role in the failure progression of specimen B.

Figure 8. AE descriptors of Specimen C classified using CNN a) Count Distribution b) Cumulative Counts c) Energy Distribution d) Cumulative Energy

Figure 8 shows the classified AE descriptors recorded from Specimen C. While looking at Figures 8a and 8c, it can be observed that despite there are some AE events with larger counts from the delamination event around 100s duration, the energies of these events are not very high. Nonetheless, the matrix cracking and delamination seems to have dominated the failure. Interestingly, the load responses in Figure 5c, shows a single load peak, which also occurs exactly around the duration of the increased energy from the matrix cracking event (Figure 8c). Similarly, the cumulative energies and cumulative counts of the matrix cracking events show a rapid increase around this same period. Therefore, it can be said that the major failure is due to the matrix cracking and the delamination event. The fibre breakage event, when compared with the other specimens in Figures 6 and 7, seem to have even lesser energy and counts in specimen C. Specimen C also seem to have higher load

peaks than the specimens A and B in Figure 5. This can lead to the conclusion that a very few delamination and significantly no debonding or bridging has occurred in specimen C, leading to a single load peak, which is higher than the other two specimens.

The AE waveforms classified using the trained CNN can effectively identify the different damage modes occurring in the mode I delamination specimens tested in this study. A point which must be addressed at this juncture is that this trained CNN while working effectively for the mode I delamination tests with the defined test configurations, must be used cautiously for other similar tests. Because the propagation of the AE waves is subjected to attenuation in both frequency and time domains, depending on the geometrical configuration and the material properties. Besides, the acquisition of the AE waves is purely based on the type of the transducing system used. Therefore, for using this CNN for classifying AE events from a different material, say adhesively bonded CFRPs or metallic specimens, the network must be retrained with a different set of input data from the desired material.

5. Conclusion

A deep convolutional neural network is developed in this study, which is trained with the acoustic emission waveforms generated from four different failure modes of CFRP specimens. The developed CNN model showed high accuracy in classifying the AE waveforms from different damage modes when the input is given as the Mel spectrograms. The pretrained model is then used for classifying failure modes from another set of mode I delamination specimens. Effectively, the classified AE waveforms can be mapped to the different damage modes during the failure progression of the test specimens. The results showed that the failure is dominated by the matrix cracking and delamination events, while there is a lack of evidence of debonding due to the bridging of the fibres. Fibre breakage events also played less significant role in the failure of the specimens. This is concurrent to the layup and loading configuration of the test specimens, there proving the efficiency of the CNN model developed. In a nutshell, the trained CNN using Mel spectrograms of the acoustic waveforms can classify the different damage modes during the failure progression of the CFRP specimens successfully.

Author Contributions

Conceptualization: Vimalathithan Paramsamy Kannan, Claudia Barile, Giovanni Pappalettera

Methodology: Vimalathithan Paramsamy Kannan, Claudia Barile, Giovanni Pappalettera

Validation: Vimalathithan Paramsamy Kannan, Claudia Barile, Giovanni Pappalettera

Formal analysis: Vimalathithan Paramsamy Kannan
Data Curation: Claudia Barile

Writing - Original Draft: Vimalathithan Paramsamy Kannan

Writing - Review & Editing: Vimalathithan Paramsamy Kannan, Claudia Barile, Giovanni Pappalettera

Supervision: Caterina Casavola

Data availability: The raw/processed data required to reproduce these findings cannot be shared at this time as the data also forms part of an ongoing study.

References

1. Fabbrocino F, Farina I, Modano M. Loading noise effects on the system identification of composite structures by dynamic tests with vibrodyne. Compos Part B-Eng. 2017;115:376-83.
2. Mancusi G, Fabbrocino F, Feo L, Fraternali F. Size effect and dynamic properties of 2D lattice materials. Compos Part-B Eng. 2017;112:235-42.
3. Darban H, Luciano R, Caporale A, Fabbrocino F. Higher modes of buckling in shear deformable nanobeams. Int J Eng Sci. 2020;154:103338.
4. De Groot PJ, Wijnen PA, Janssen RB. Real-time frequency determination of acoustic emission for different fracture mechanisms in carbon/epoxy composites. Compos Sci Tech. 1995;55(4):405-12.
5. Wisnom MR. Size effects in the testing of fibre-composite materials. Compos Sci Tech. 1999;59(13):1937-57.
6. Sause MG. Failure of fiber-reinforced composites. InIn Situ Monitoring of Fiber-Reinforced Composites 2016 (pp. 5-55). Springer, Cham.
7. Barile C, Casavola C, Pappalettera G, Kannan VP. Application of different acoustic emission descriptors in damage assessment of fiber reinforced plastics: A comprehensive review. Eng Fract Mech. 2020;235:107083.
8. Hamstad MA. A review: acoustic emission, a tool for composite-materials studies. Exp Mech. 1986;26(1):7-13.
9. Saeedifar M, Zarouchas D. Damage characterization of laminated composites using acoustic emission: A review. Compos Part B-Eng. 2020;195:108039.

10. Sause MG, Horn S. Simulation of acoustic emission in planar carbon fiber reinforced plastic specimens. J Nondest Eval. 2010;29(2):123-42.

11. Oz FE, Ersoy N, Lomov SV. Do high frequency acoustic emission events always represent fibre failure in CFRP laminates? Compos Part A-Appl Sci. 2017 Dec 1;103:230-5.

12. Hamstad MA. Thirty years of advances and some remaining challenges in the application of acoustic emission to composite materials. Acoustic emission beyond the millennium. 2000:77-91.

13. De Groot PJ, Wijnen PA, Janssen RB. Real-time frequency determination of acoustic emission for different fracture mechanisms in carbon/epoxy composites. Compos Sci Tech. 1995;55(4):405-12.

14. Barile C, Casavola C, Pappalettera G, Vimalathithan PK. Damage characterization in composite materials using acoustic emission signal-based and parameter-based data. Compos Part B-Eng. 2019 Dec 1;178:107469.

15. Sadowski L. Non-destructive investigation of corrosion current density in steel reinforced concrete by artificial neural networks. Arch Civil Mech Eng. 2013;13(1):104-11.

16. Meng M, Chua YJ, Wouterson E, Ong CP. Ultrasonic signal classification and imaging system for composite materials via deep convolutional neural networks. Neurocomputing. 2017;257:128-35.

17. Cha YJ, Choi W. Büyüköztürk O. Deep learning-based crack damage detection using convolutional neural networks. Comput-Aid Civ Inf. 2017;32(5):361-378.

18. Nasiri A, Bao J, Mccleeary D, Louis SY, Huang X, Hu J. Online Damage Monitoring of SiC f-SiC m Composite Materials Using Acoustic Emission and Deep Learning. IEEE Access. 2019;7:140534-41.

19. Lin YZ, Nie ZH, Ma HW. Structural damage detection with automatic feature-extraction through deep learning. Comput-Aid Civ Inf. 2017;32(12):1025-46.

20. McCrory JP, Al-Jumaili SK, Crivelli D, Pearson MR, Eaton MJ, Featherston CA, Guagliano M, Holford KM, Pullin R. Damage classification in carbon fibre composites using acoustic emission: A comparison of three techniques. Compos Part-B: Eng. 2015;68:424-30.

21. Sikdar S, Liu D, Kundu A. Acoustic emission data based deep learning approach for classification and detection of damage-sources in a composite panel. Composites Part B: Engineering. 2022;228:109450.

22. Khan A, Ko DK, Lim SC, Kim HS. Structural vibration-based classification and prediction of delamination in smart composite laminates using deep learning neural network. Compos Part B-Eng. 2019;161:586-94.

23. Lu L, Wang X, Carneiro G, Yang L, editors. Deep learning and convolutional neural networks for medical imaging and clinical informatics. Springer International Publishing; 2019 Sep 19.

24. Venkatesan R, Li B. Convolutional neural networks in visual computing: a concise guide. CRC Press; 2017.

25. Krizhevsky A, Sutskever I, Hinton G.E. Imagenet classification with deep convolutional neural networks. Adv Neur In. 2012;25.

26. Goodfellow I, Bengio Y, Courville A. Deep learning. MIT press; 2016.

27. He K, Zhang X, Ren S, Sun J. Delving deep into rectifiers: Surpassing human-level performance on imagenet classification. InProceedings of the IEEE international conference on computer vision 2015 (pp. 1026-1034).

28. https://uk.mathworks.com/products/deep-learning.html (last accessed on July 19, 2021)

29. https://uk.mathworks.com/help/deeplearning/ref/nnet.cnn.trainingoptionssgdm.html (last accessed on July 19, 2021)

30. Shen J, Pang R, Weiss RJ, Schuster M, Jaitly N, Yang Z, Chen Z, Zhang Y, Wang Y, Skerrv-Ryan R, Saurous RA. Natural tts synthesis by conditioning wavenet on mel spectrogram predictions. In2018 IEEE International Conference on Acoustics, Speech and Signal Processing (ICASSP) 2018 Apr 15 (pp. 4779-4783). IEEE.

31. Meng H, Yan T, Yuan F, Wei H. Speech emotion recognition from 3D log-mel spectrograms with deep learning network. IEEE access. 2019 Aug 28;7:125868-81.

32. Narayanan A, Wang D. Ideal ratio mask estimation using deep neural networks for robust speech recognition. In2013 IEEE International Conference on Acoustics, Speech and Signal Processing 2013 May 26 (pp. 7092-7096). IEEE.

33. Medina R, Cerrada M, Cabrera D, Sánchez RV, Li C, De Oliveira JV. Deep learning-based gear pitting severity assessment using acoustic emission, vibration and currents signals. In2019 Prognostics and System Health Management Conference (PHM-Paris) 2019 May 2 (pp. 210-216). IEEE.

34. Chuang WY, Tsai YL, Wang LH. Leak detection in water distribution pipes based on CNN with mel frequency cepstral coefficients. InProceedings of the 2019 3rd International Conference on Innovation in Artificial Intelligence 2019 Mar 15 (pp. 83-86).

35. Barile C, Casavola C, Pappalettera G, Vimalathithan PK. Experimental wavelet analysis of acoustic emission signal propagation in CFRP. Eng Fract Mech. 2019;210:400-7.

36. ASTM D5528-13, Standard Test Method for Mode I Interlaminar Fracture Toughness of Unidirectional Fiber-Reinforced Polymer Matrix Composites, ASTM International, West Conshohocken, PA, 2013, www.astm.org

37. Gillis PP. Dislocation motions and acoustic emissions. InAcoustic Emission 1972 Jan. ASTM International.

38. Finkel P, Mitchell JR, Carlos MF. Experimental study of "Auto Sensor Test–Self Test Mode" for Acoustic Emission system performance verification. InAIP Conference Proceedings 2000 May 23 (Vol. 509, No. 1, pp. 1995-2002). American Institute of Physics.

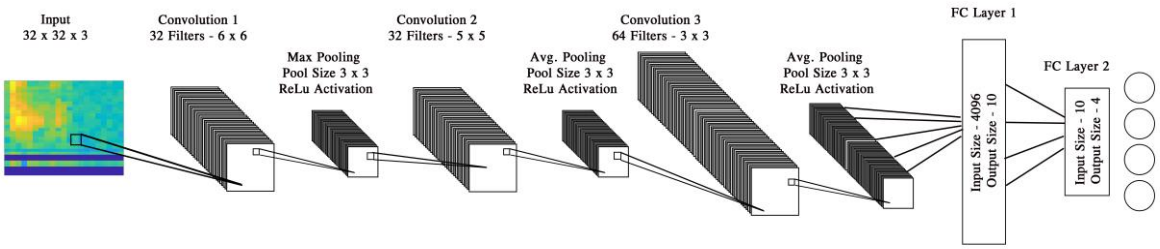

Figure 1. Architecture of the Convolutional Neural Network

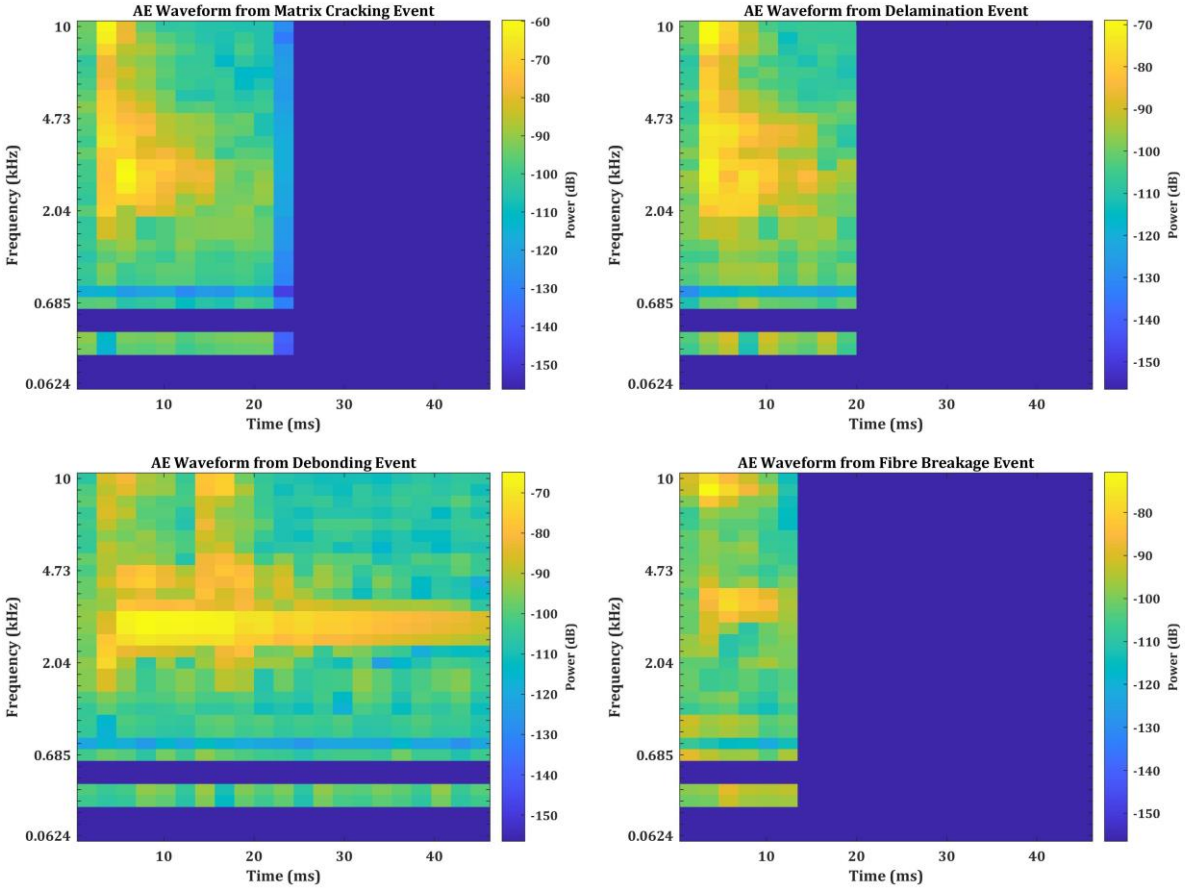

Figure 2. Mel Spectrograms of representative waveforms from Matrix Cracking, Delamination, Debonding and Fibre Breakage events

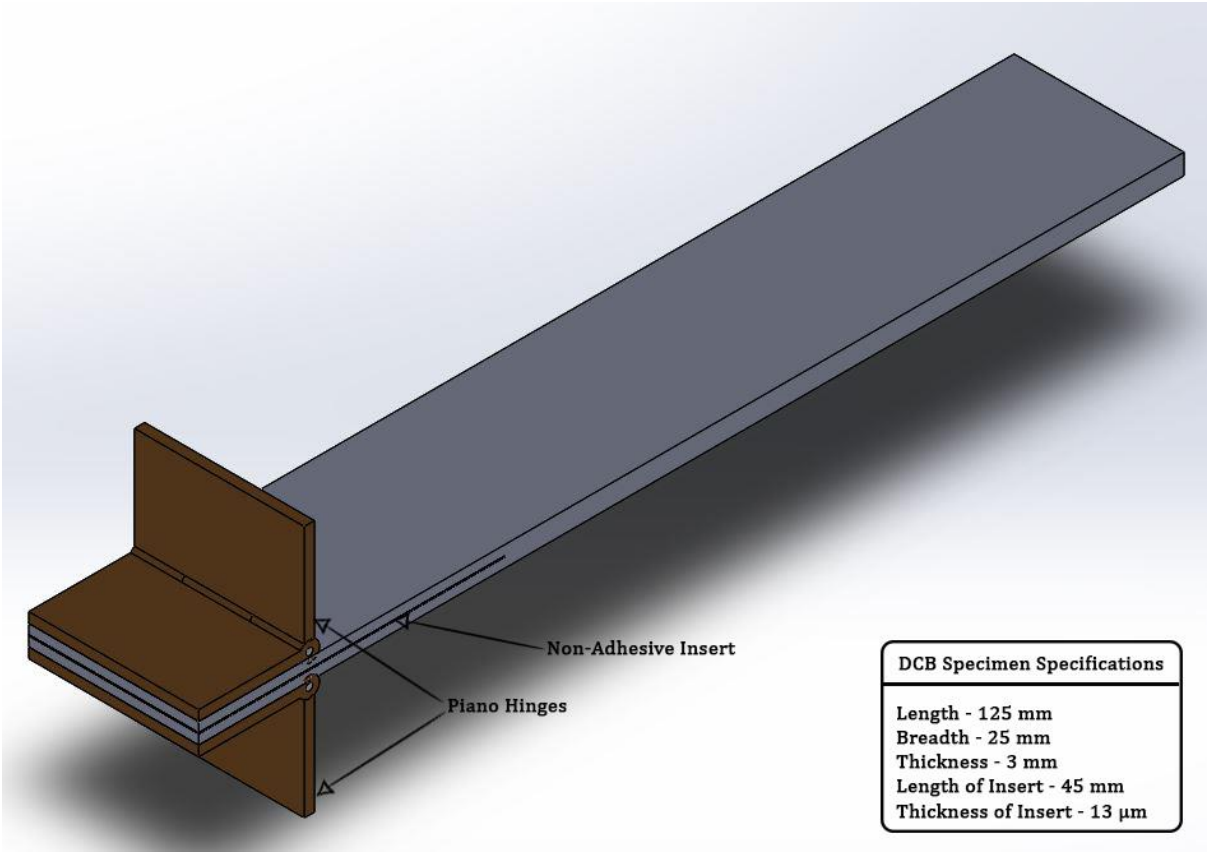

Figure 3. Schematic of the test specimen

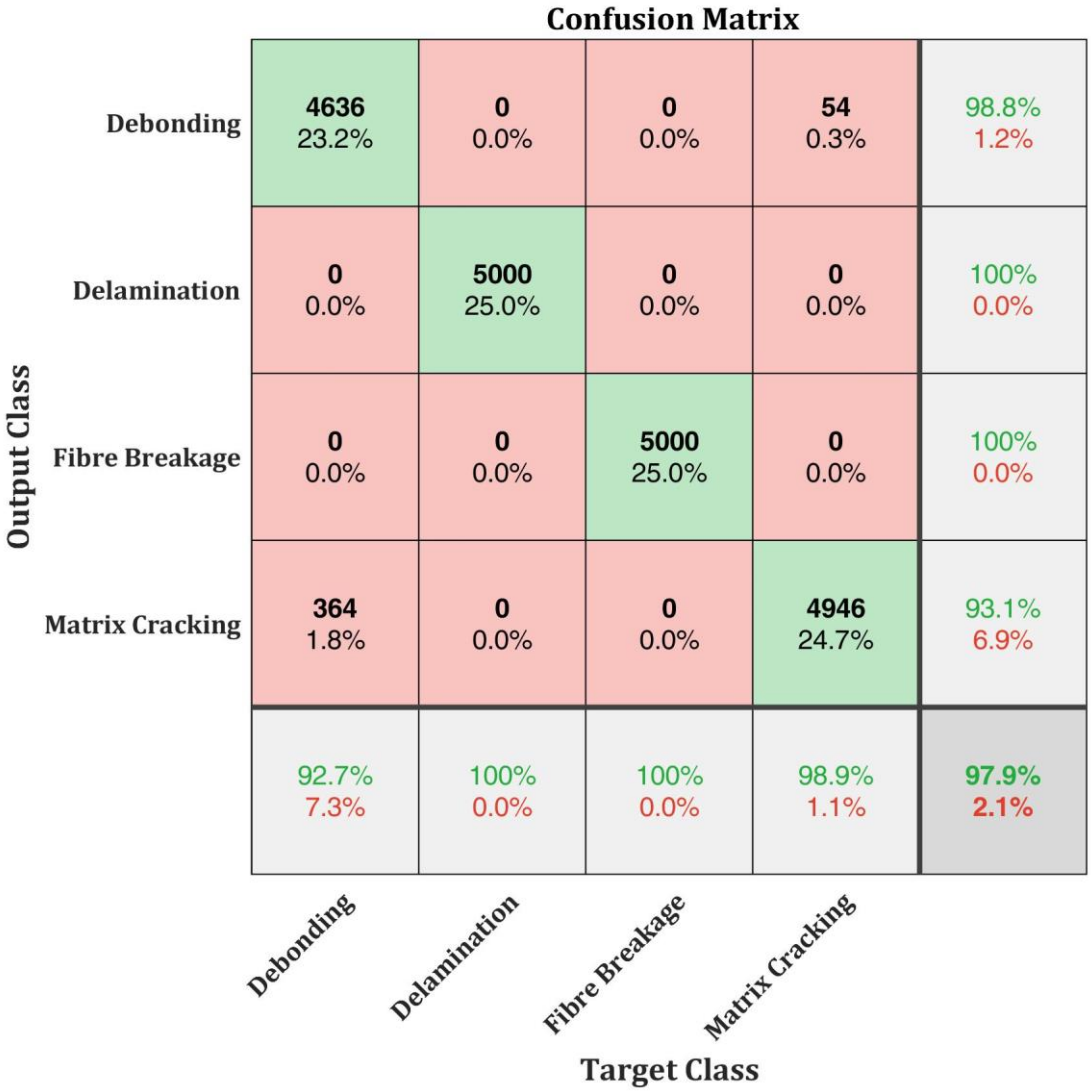

Figure 4. Confusion Matrix of the CNN classifying the damage modes

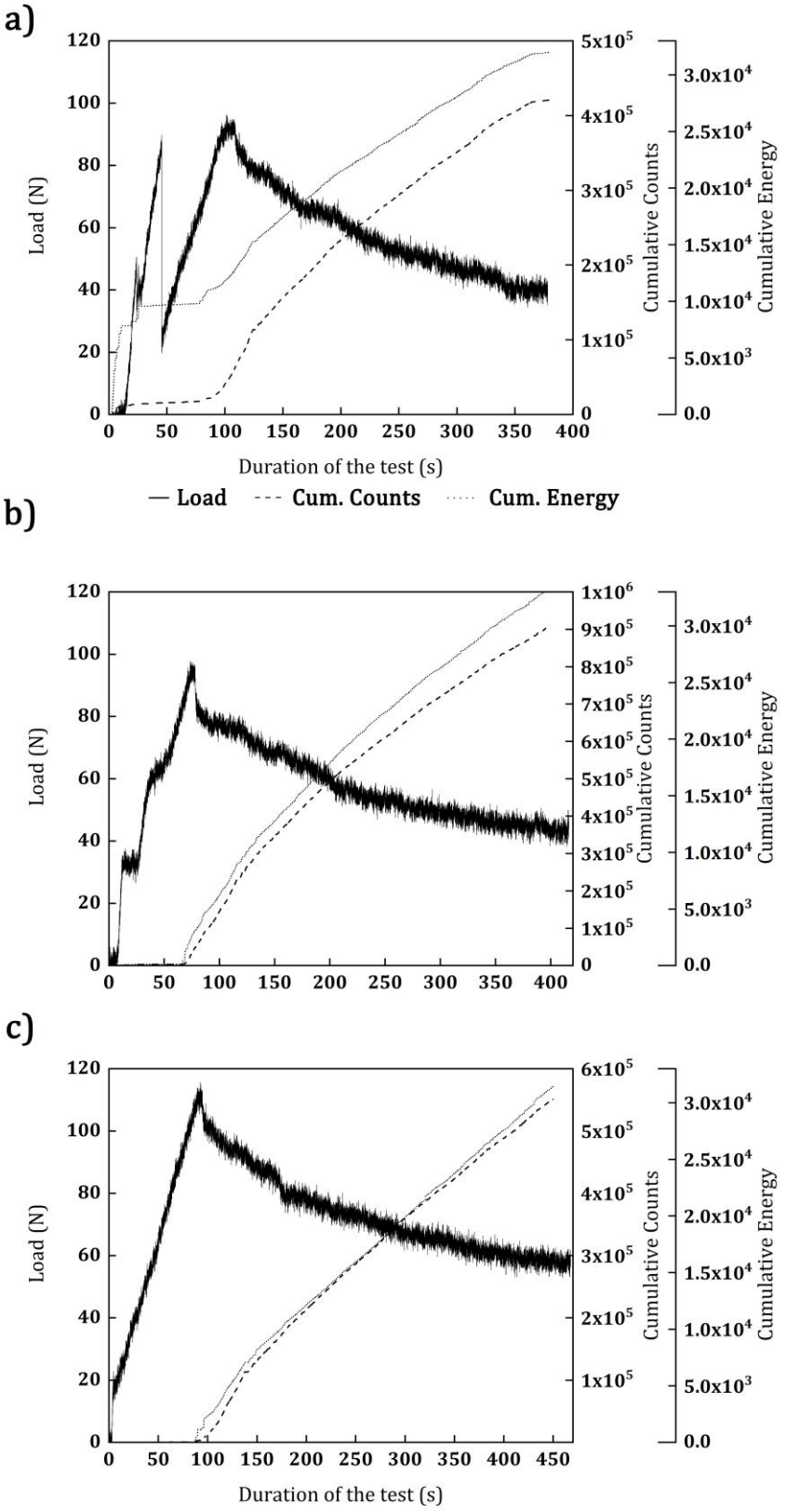

Figure 5. Load Responses, Cumulative Counts and Cumulative Energy of the Acoustic Events for a) Specimen A, b) Specimen b and c) Specimen C

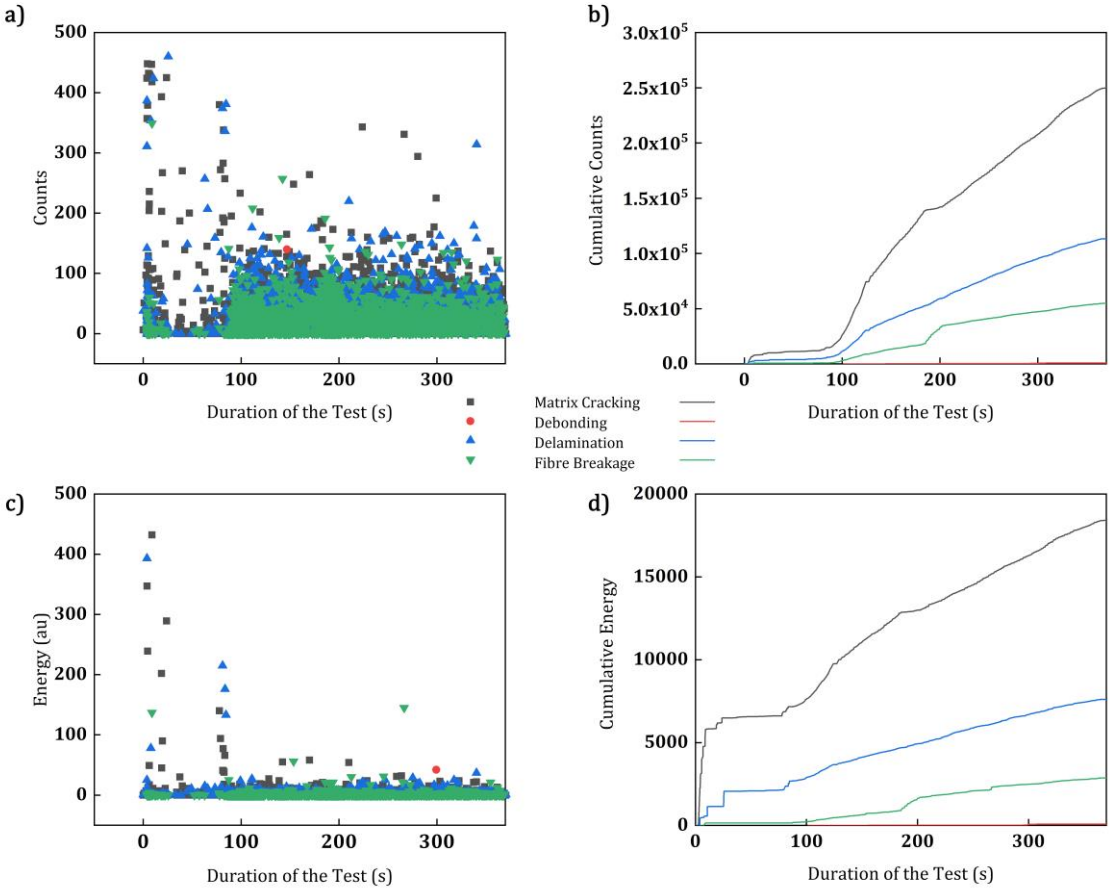

Figure 6. AE descriptors of Specimen A classified using CNN a) Count Distribution b) Cumulative Counts c) Energy Distribution d) Cumulative Energy

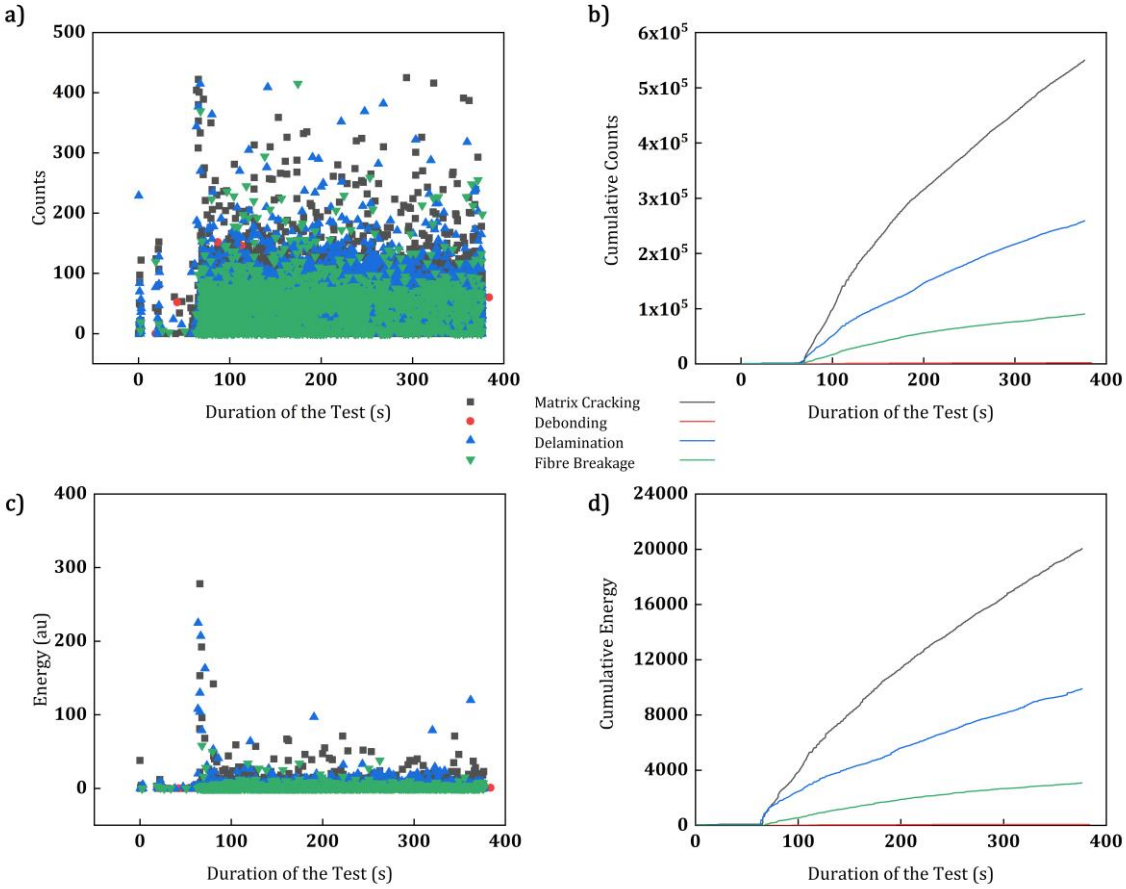

Figure 7. AE descriptors of Specimen B classified using CNN a) Count Distribution b) Cumulative Counts c) Energy Distribution d) Cumulative Energy

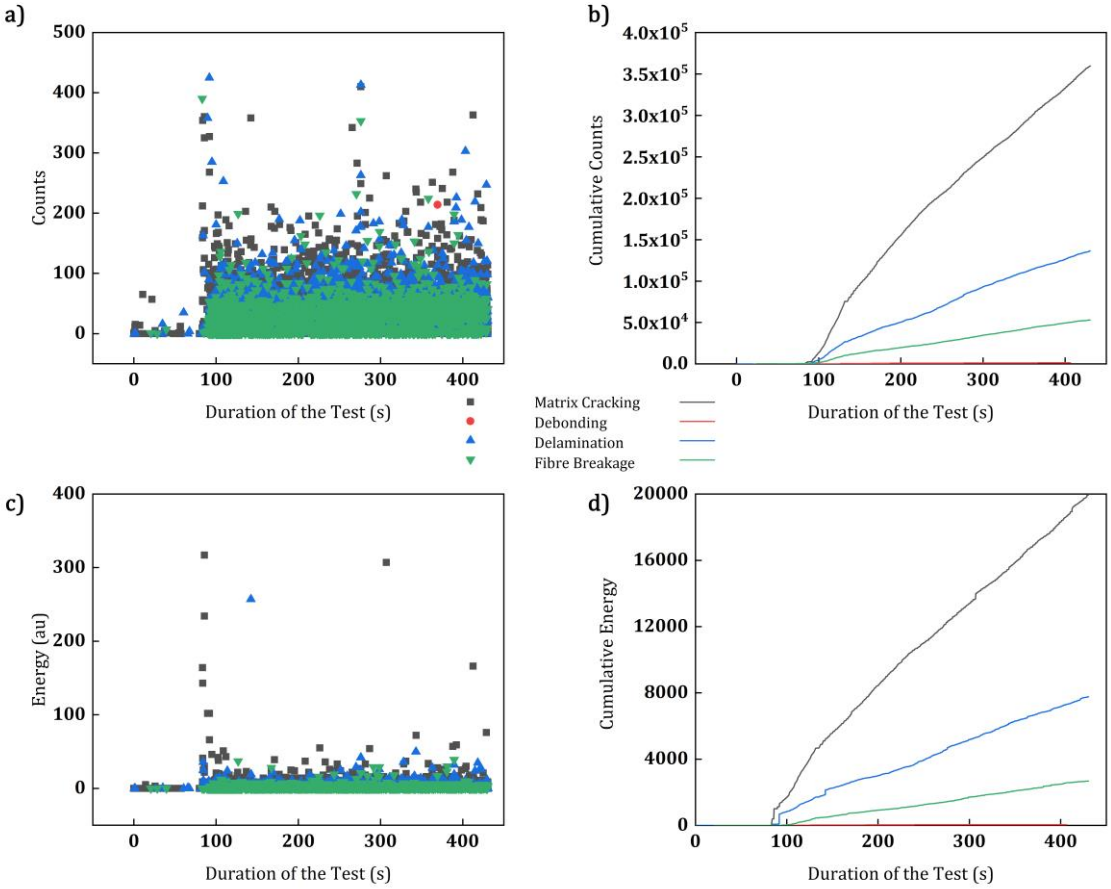

Figure 8. AE descriptors of Specimen C classified using CNN a) Count Distribution b) Cumulative Counts c) Energy Distribution d) Cumulative Energy

Table 1. Configuration of the Proposed CNN model

Layer Name	Layer Description
Input Layer	32 x 32 x 3 Spectrogram
Convolutional Layer 1 (Conv 1)	Number of Filters: 32 Filter Size: 6 x 6 Stride: 1; Padding 2
Pooling Layer	Max Pooling Layer Pool Size: 3 x 3 Stride: 2; Padding 2 ReLu Activation
Convolutional Layer 2 (Conv 2)	Number of Filters: 32 Filter Size: 5 x 5 Stride: 1; Padding 2
Pooling Layer	Average Pooling Layer Pool Size: 3 x 3 Stride: 1; Padding: 2 ReLu Activation
Convolutional Layer 3 (Conv 3)	Number of Filters: 64 Filter Size: 5 x 5 Stride: 1; Padding 2
Pooling Layer	Average Pooling Layer Pool Size: Stride: 2; Padding: 2 ReLu Activation
Fully Connected Layer	Input Size: 576 Output Size: 64 ReLu Activation
Fully Connected Layer	Input Size: 64 Output Size: 4
Softmax Layer	-
Classification Layer	-

Table 2. AE waveforms recorded from the CFRP test specimens under Mode I Delamination

Specimen Name	Number of AE Waveforms recorded
A	19865
B	19492
C	20799